Supplementary Information: Distinct Solvation patterns of OH^- versus H_3O^+ charge defects at electrified gold/water interfaces govern their properties

Chanbum Park,[1] Soumya Ghosh,[1,2] Harald Forbert[3] and Dominik Marx[1]

[1]Lehrstuhl für Theoretische Chemie, Ruhr-Universität Bochum, 44780 Bochum, Germany
[2]Present address: Tata Institute of Fundamental Research Hyderabad, Hyderabad, Telangana 500046, India
[3]Center for Solvation Science ZEMOS, Ruhr-Universität Bochum, 44780 Bochum, Germany
chanbum.park@theochem.ruhr-uni-bochum.de

1 Potentiostat

To apply electrochemical bias across the cell during the AIMD simulations, we employ an electrochemical cell method,[1] where the voltage is obtained from the dipole correction [2] at the center of the vacuum between a computational counter electrode (Ne in this case) and the bottomost layer of the electrode of interest (Au). This voltage is a direct measure of the electrode potential at the Au/water interface. In this method, the effective nuclear charge of the Ne atoms of the computational counter electrode is modified to charge the electrode of interest; we refer the interested reader to Ref. [1] for background, validation and details of this method. By increasing (or decreasing) the effective nuclear charge of each Ne atom from Z_{Ne} to $Z_{\mathrm{Ne}} + \sigma/n$, where σ and n are the net excess charge and the total number of Ne atoms respectively, additional electrons (or electron holes) are created at the conduction band (or valence band) of the Ne atoms to conserve the net charge; note that σ does not need to be integer and thus allows one to continuously change the bias. The additional electrons in the conduction band are redistributed to the Au electrode during electronic structure calculations since the conduction band minimum of the Ne is much higher than the Fermi level. For electron holes, electrons from the Au electrode are accumulated in the valence band of the Ne atoms. In the actual implementation, instead of balancing the number of electrons on each species according to their modified effective nuclear charge, the occupation number of the orbitals are modified according to the net excess charge, σ. This net transfer of electrons, with reference to the isolated species, generates an electric field between the electrodes with the surface charge σ. The charged electrode attracts or repels water molecules and ions. The ensuing distributions of ions and oriented water molecules at the Au surface cause potential drops across the cell. The potential drop is compensated by a dipole correction in the middle of the vacuum region so that there is no net dipole across the simulation cell.[2] This allows one to compute the instantaneous voltage within the cell as well as the overall periodic variation of the potential.

To reach the target potential, the core charge of the Ne atoms is updated according to the target voltage and the current voltage. The additional charge σ_{add} to maintain the target voltage is determined as[1] $\sigma^{\mathrm{add}} = \beta(V^{\mathrm{target}} - V^{\mathrm{Aver.}})$, where the value of β is chosen to be 1 eV^{-1} while the maximum possible charge update value is set to 0.01 e. In practice, the current (instantaneous) voltage is averaged over 200 fs of AIMD simulation, denoted as $V^{\mathrm{Aver.}}$, and compared with the target voltage V^{target} to update σ^{add} accordingly. Following the protocol validated in Ref. [1], a fraction of the snapshots were used to compute the achieved averaged potential $V^{\mathrm{Aver.}}$ as

$$V^{\mathrm{Aver.}} = \sum_{i>\alpha N_0}^{N_0} V(i)/(N_0 - \alpha N_0), \tag{1}$$

where $V(i)$ is the current potential at snapshot i and N_0 is the number of steps for each run (200 fs).

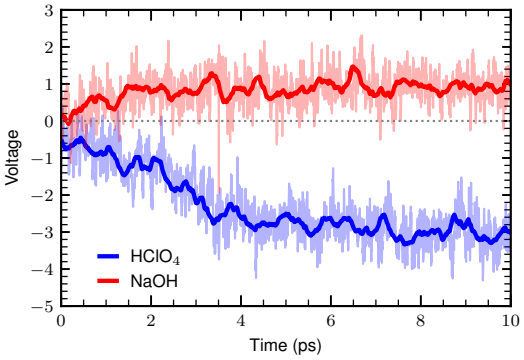

Supplementary Figure 1: Evolution of the instantaneous voltages (light colors) and the averaged voltages (thick lines) for the acidic ($HClO_4$) and alkaline (NaOH) systems as a function of AIMD sampling.

We set $\alpha = 0.8$ and the target potential drop is increased/decreased every 200 fs by $\pm$ 0.2 V.

2 Collective variables to define the charge defects

Inspired by previous work [3], collective variables (CVs) are used to trace the positions of the H_3O^+ and OH^- charge defects using a in-house modified version of CP2K. The CV of the position of H_3O^+ or OH^- is computed from

$$s = \frac{\sum_{i \in O_w} z_i \exp(\lambda n_i)}{\sum_{i \in O_w} \exp(\lambda n_i)}, \tag{2}$$

where λ is a large constant (with values of 20 and -20 for the acid and alkaline systems, respectively), O_w are the oxygen atoms and z_i are the positions of these O_w atoms on the z-axis. The number of hydrogen atoms n_i around an O atom i is computed from

$$n_i = \sum_{j \in H} n^H(r_{ij}), \tag{3}$$

where $n^H(r)$ is a continuous function to count the number of H atoms around O atoms,

$$n^H(r_{ij}) = \frac{1 - (r_{ij}/r_c)^8}{1 - (r_{ij}/r_c)^{16}}, \tag{4}$$

where r_{ij} is the distance between O and H atoms, and r_c is a cutoff radius (set to 1.27 and 1.11 Å for H_3O^+ and OH^-, respectively). This parameterization provides $n_i \approx 2$ for intact water molecules, ≈ 1 for OH^-, and ≈ 3 for H_3O^+ as required.

We use these CVs to tag and to track the two charge defects (as depicted for instance in Figure 1(c) in the main text) and to apply the mechanical wall potential in case of H_3O^+ to keep this defect close to the gold electrode at zero bias (see Supplementary Figure 3).

3 Radial distribution functions in a slab geometry

Since solid/liquid interfaces are inhomogeneous and anisotropic in the z-direction versus the xy-plane, conventional spherical radial distribution functions (RDFs) cannot be used to quantify the particle distributions. Hence, we normalize the RDFs using a cylindrical volume instead following previous work [4–6]

$$g_{i,j}(r) = \frac{\rho_j(r)}{\rho} = \frac{n_{i,j}(r)}{2\pi r h \mathrm{d}r}, \tag{5}$$

where ρ is the density in the slab, $\rho_j(r)$ is the density of atom j at a distance r around atom i, $n(i,j)(r)$ is the number of j atoms at a distance between r and $r + \mathrm{d}r$, and h is the width of the slab.

4 Trajectories of H_3O^+

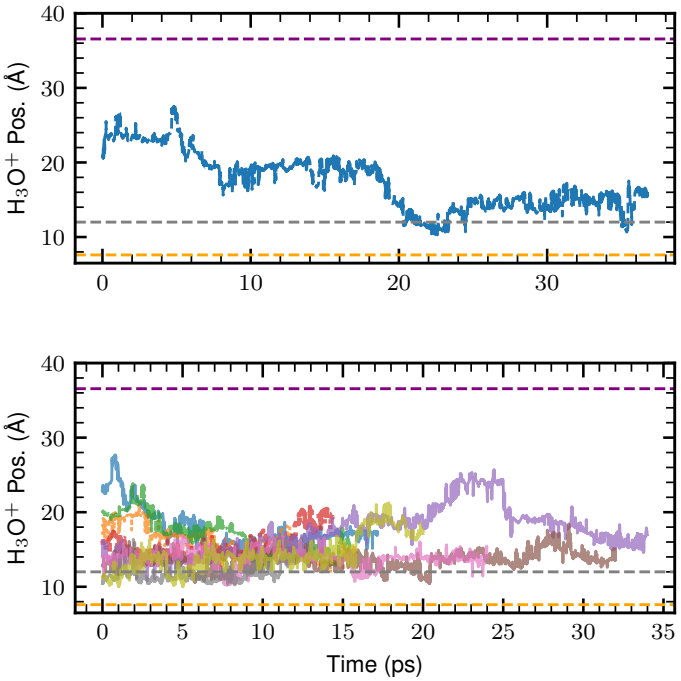

Supplementary Figure 2: H_3O^+ positions at finite bias of -3 V. The trajectory in the upper panel was monitored from the beginning of the charging stage. Additional trajectories in the lower panel were launched with new velocities of atoms after the trajectory in the upper panel reached about -3 V. Purple, gray, and orange horizontal dashed lines indicate the positions of the Ne electrode, the first water layer (the interface region IF, see main text), and the average top Au layer, respectively.

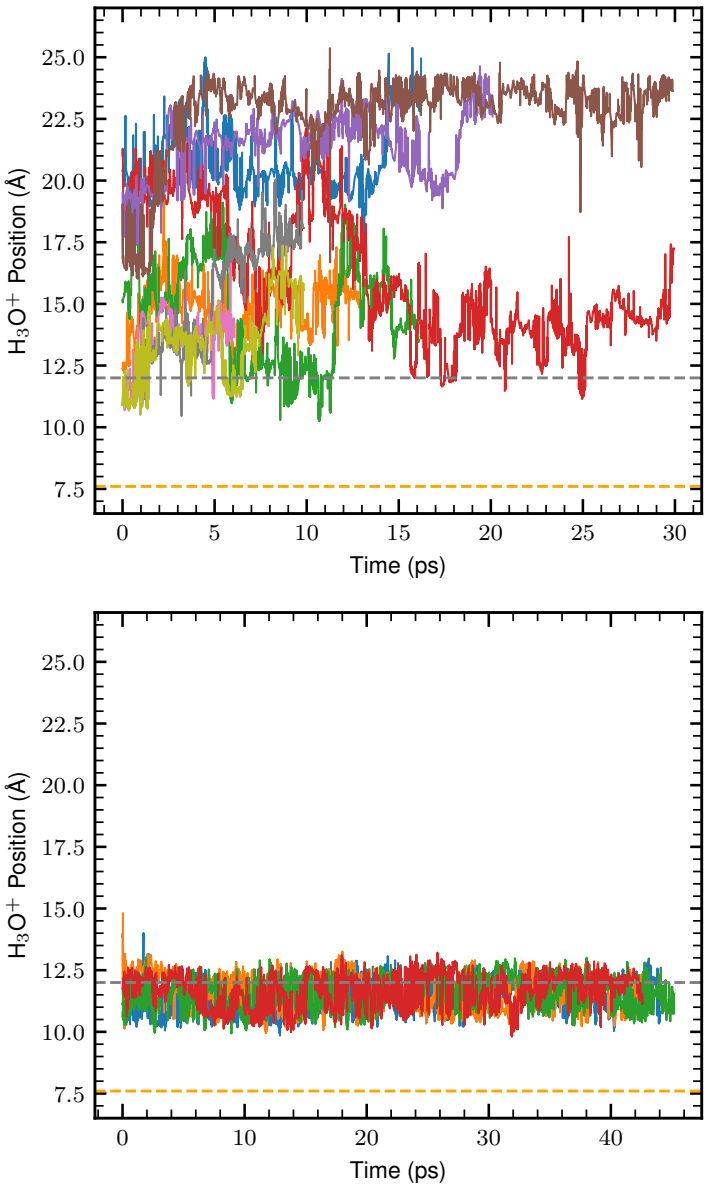

Supplementary Figure 3: Positions of H_3O^+ without bias potentials while applying a mechanical wall potential acting on H_3O^+ at 24 Å (upper panel) and 12 Å (lower panel), respectively, to force H_3O^+ to undergo Grotthuss-type charge migration in some proximity of the Au surface. Gray and orange horizontal dashed lines indicate the positions of the first water layer (the interface region IF, see main text), and the average top Au layer, respectively. Note the different position scale compared to Supplementary Figure 2.

5 Angles

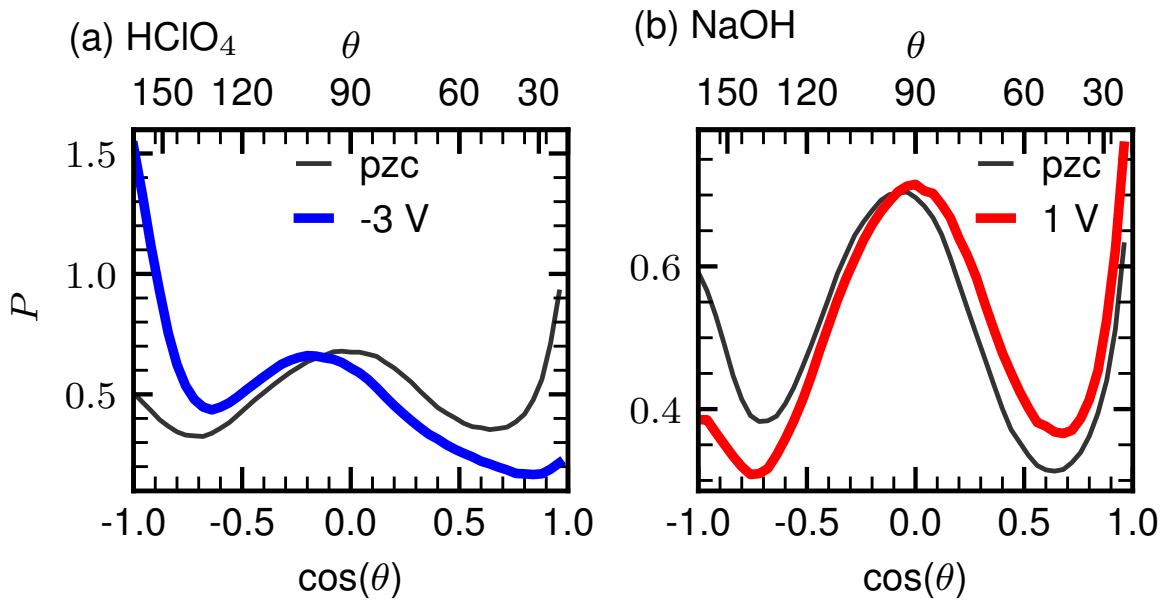

Supplementary Figure 4: Probability distributions of the angle θ of OH vectors of water molecules in the (a) acidic ($HClO_4$) and (b) alkaline (NaOH) (b) electrolytes systems.

6 Trajectories and density profiles of OH^-

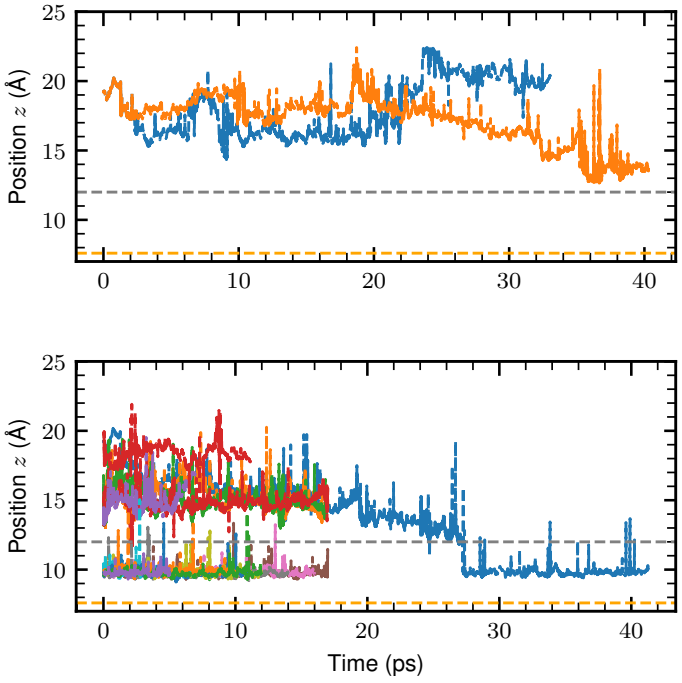

Supplementary Figure 5: Positions of OH^- at finite bias of 1 V. The trajectories in the upper panel were monitored from the beginning of the charging stage. Additional trajectories in the lower panel were launched with new velocities of atoms after the trajectories in the upper panel reached about 1 V. Gray, and orange horizontal dashed lines indicate the positions of the first water layer (the interface region IF, see main text), and the average top Au layer, respectively. Note the different position scale compared to Supplementary Figure 2.

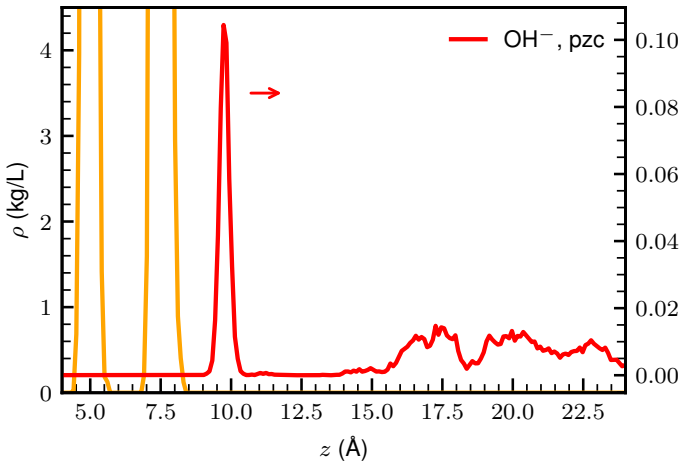

Supplementary Figure 6: Density profile of OH^- without applying bias potentials.

7 Net atomic charges

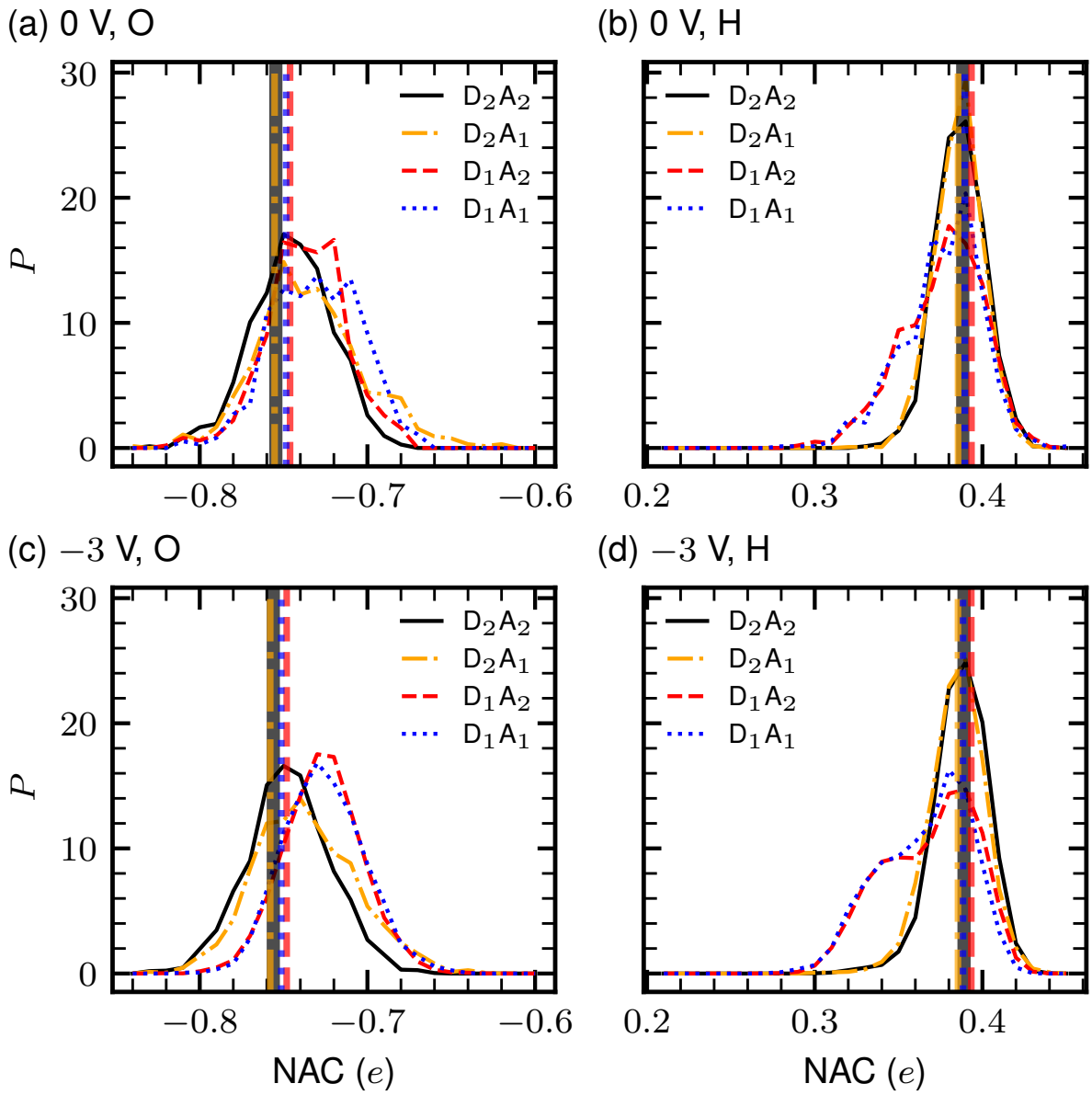

Supplementary Figure 7: Net atomic charges (NAC) of oxygen (O) and hydrogen (H) atoms in water molecules depending on their hydrogen bonding state in the $HClO_4$ system. The vertical lines correspond to the values in the bulk-like (BL) region. The hydrogen bond patterns of water molecules are denoted as D_nA_m where n and m are the number of donor and acceptor bonds, respectively.

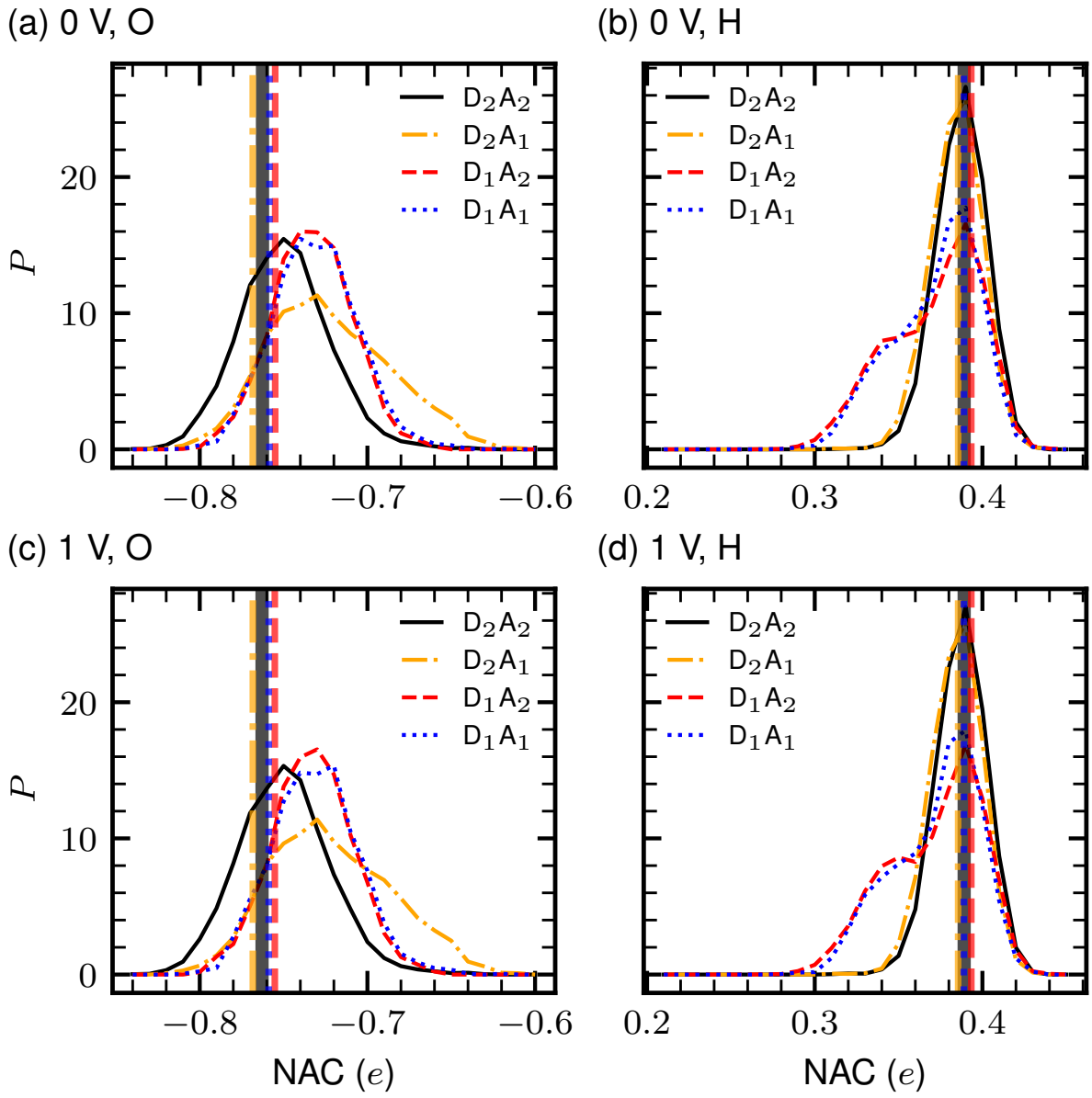

Supplementary Figure 8: Net atomic charges (NAC) of oxygen (O) and hydrogen (H) atoms in water molecules depending on their hydrogen bonding state in the NaOH system. The vertical lines correspond to the values in the bulk-like (BL) region. The hydrogen bond patterns of water molecules are denoted as D_nA_m where n and m are the number of donor and acceptor bonds, respectively.

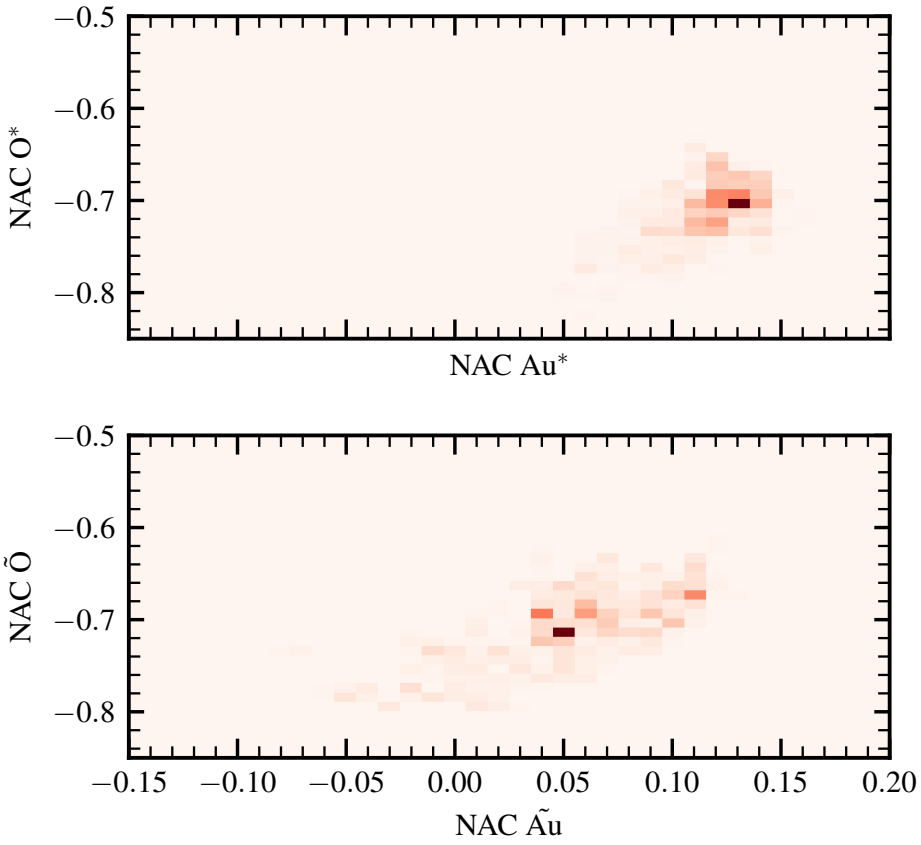

Supplementary Figure 9: NAC distributions of O^* as a function of Au^* (upper panel) and $\tilde{O}$ as a function of $\tilde{Au}$ (lower panel) at finite bias of 1 V; see main text for atom labeling.

Supplementary Table 1: Donor and acceptor numbers of OH^- for the alkaline system (NaOH) with/without a bias potential. The resting state is defined based on the charge transfer coordinate δ as $|\delta| > 0.5$ where $\delta = d_{O^*-H^*} - d_{\tilde{O}-H^*}$ while the active state is defined as $|\delta| < 0.1$.

Voltage (V)	HB status	IF		IM		BL	
		Resting	Active	Resting	Active	Resting	Active
0	Donor	0.83	0.91	0.70	0.87	0.75	0.84
	Acceptor	2.74	2.60	4.41	3.58	4.43	3.80
1	Donor	0.87	0.95	0.81	0.85	0.84	0.85
	Acceptor	2.83	2.42	4.52	3.96	4.76	3.91

References

1. Surendralal, S., Todorova, M., Finnis, M. W. & Neugebauer, J. First-principles approach to model electrochemical reactions: Understanding the fundamental mechanisms behind Mg corrosion. *Rev. Lett.* **120,** 246801 (2018).
2. Neugebauer, J. & Scheffler, M. Adsorbate-substrate and adsorbate-adsorbate interactions of Na and K adlayers on Al (111). *Phys. Rev. B* **46,** 16067 (1992).
3. Park, J. M., Laio, A., Iannuzzi, M. & Parrinello, M. Dissociation mechanism of acetic acid in water. *J. Am. Chem. Soc.* **128,** 11318–11319 (2006).
4. Schoen, M., Diestler, D. & Cushman, J. Fluids in micropores. I. Structure of a simple classical fluid in a slit-pore. *J. Chem. Phys.* **87,** 5464–5476 (1987).
5. Das, B., Sharma, B. & Chandra, A. Effects of tert-butyl alcohol on water at the liquid–vapor interface: Structurally bulk-like but dynamically slow interfacial water. *J. Phys. Chem. C* **122,** 9374–9388 (2018).
6. Goujon, F., Malfreyt, P. & Tildesley, D. The pair distribution function in the planar gas–liquid interface: Application to the calculation of the surface tension. *J. Chem. Phys.* **151** (2019).